

Identifying Entanglement Phases with Bipartite Projected Ensembles

Zi-Yong Ge¹ and Franco Nori (野理)^{1,2,3}

¹Theoretical Quantum Physics Laboratory, Cluster for Pioneering Research, RIKEN, Wako-shi, Saitama 351-0198, Japan

²Quantum Information Physics Theory Research Team,

Center for Quantum Computing, RIKEN, Wako-shi, Saitama 351-0198, Japan

³Department of Physics, University of Michigan, Ann Arbor, Michigan 48109-1040, USA

We introduce bipartite projected ensembles (BPEs) for quantum many-body wave functions, which consist of pure states supported on two local subsystems, with each state associated with the outcome of a projective measurement of the complementary subsystem in a fixed local basis. We demonstrate that the corresponding ensemble-averaged entanglements (EAEs) between two subsystems can effectively identify entanglement phases. In volume-law entangled states, EAE converges to a nonzero value with increasing distance between subsystems. For critical systems, EAE exhibits power-law decay, and it decays exponentially for area-law systems. Thus, entanglement phase transitions can be viewed as a disorder-order phase transition. We also apply BPE and EAE to measured random Clifford circuits to probe measurement-induced phase transitions. We show that EAE serves not only as a witness to phase transitions, but also unveils additional critical phenomena properties, including dynamical scaling and surface critical exponents. Our findings provide an alternative approach to diagnosing entanglement laws, thus enhancing the understanding of entanglement phase transitions. Moreover, given the scalability of measuring EAE in quantum simulators, our results hold promise for impacting quantum simulations.

Introduction.—The development of quantum information [1–4] has highlighted the significance of entanglements in understanding quantum matter [4–6]. For instance, in local gapped quantum many-body systems, the entanglement entropies of ground states conform to the area law [7]. However, in critical systems, the entanglement entropies display logarithmic divergence [8–11]. In addition to low-energy physics, entanglements can also shed light on non-equilibrium quantum phases [12]. Specifically, the singular changes of entanglement dynamics in quantum many-body systems can be identified by entanglement phase transitions. A novel family of entanglement phase transitions, known as measurement-induced phase transitions (MIPTs) [13–36], has been discovered in monitored quantum many-body systems, and is currently under experimental investigation in various quantum simulators [37–39]. The different measurement-induced phases manifest in different behaviors of entanglements in steady states. For small rates of measurements, the system resides in an entangling phase with volume-law entanglements of steady states. For high measurement rates, it is disentangling phase with area-law entanglements. At the critical point, the steady states generally exhibit logarithmic entanglement entropies, satisfying the sub-volume law.

In quantum-simulation experiments [40–42], identifying entanglement phases is always challenging. This requires state tomography or random measurements [43], both of which are difficult to scale up. Therefore, a natural question arises: Can we bypass entanglement entropies and define an experiment-friendly quantity to characterize entanglement phases? Moreover, it has been reported that entanglement dynamics in some random circuits can be mapped to classical statistical mechanics, where the entanglement entropies correspond to free energies [18, 19]. In conventional phase transitions, we generally need to define the corresponding correlation functions to identify short- and long-range order. However, no similar correlation function effectively describes the

entanglement phase transition. Thus, another open question is whether we can define a correlation function to further understand entanglement phase transitions.

In this Letter, we introduce bipartite projected ensembles (BPEs) in quantum many-body systems to investigate entanglement phases. Here, BPE is a set of pure states supported on two local subsystems, where each element represents an output state obtained after a projective measurement of the complementary subsystem in a fixed local basis. We also define ensemble-averaged entanglements (EAEs) between these two subsystems, which can be regarded as a type of correlation function. We show that the scaling of EAEs can identify the entanglement laws of quantum many-body wave functions. In the case of volume-law entanglements, EAE converges to a nonzero value for large distances between two subsystems. In a critical system, EAE follows power-law decay; whereas in an area-law system, it exhibits exponential decay. We then apply BPE and EAE to investigate the MIPT in a random Clifford circuit with local projective measurements. Our results demonstrate that EAE can effectively witness MIPT and reveal additional properties of the critical phenomena, including the universal scaling of dynamics and surface critical exponents.

Set-up.—Here, BPE is generalized from projective ensembles in Refs. [44–46]. Without loss of generality, we consider a many-qubit system, where the system is divided into three parts A, B and R with the number of qubits N_A , N_B and N_R . The local bases of each qubit are labeled by $|z\rangle$ with $z = 0, 1$, and $|\Psi\rangle$ denotes the wave function of the full system. Here, the BPE of A and B is generated by performing projective measurements on all qubits in R with a local basis $\{|z_R\rangle\}$, where $|z_R\rangle \in \{0, 1\}^{N_R}$ are the measurement results of R with probability $p(z_R)$, see Fig. 1(a). Thus, the wave function $|\Psi\rangle$ can

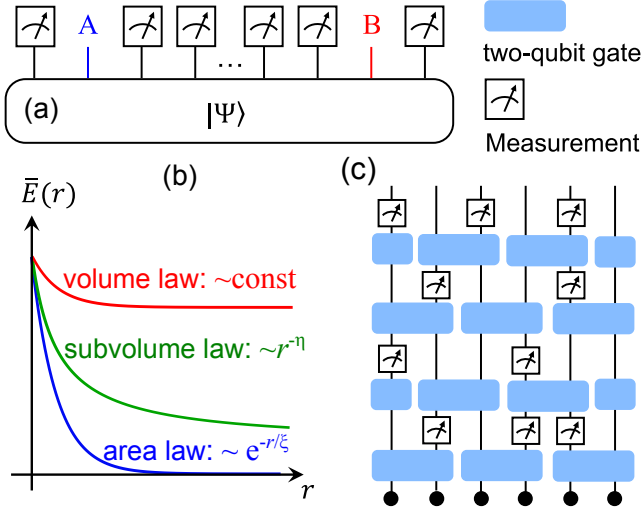


FIG. 1. Set-up. (a) The diagram of BPE. For a many-qubit system with a pure state $|\Psi\rangle$, the subsystem R is measured in a fixed local basis. Then, the remaining unmeasured subsystems A and B are in a pure state, which depends on the measurement outcome on R. (b) The scaling of EAE for different entanglement laws. (c) The structure of the unitary-measurement hybrid circuit. The local two-qubit gates are drawn from the uniformly sampled Clifford group, and the random projected measurement is onto the z -component with a probability p .

be rewritten as $|\Psi\rangle = \sum_{z_R} \sqrt{p(z_R)} |\Psi_{AB}(z_R)\rangle \otimes |z_R\rangle$ with

$$p(z_R) = \langle \Psi | (\mathbb{I}_{AB} \otimes |z_R\rangle \langle z_R|) | \Psi \rangle, \quad (1)$$

$$|\Psi_{AB}(z_R)\rangle = (\mathbb{I}_{AB} \otimes |z_R\rangle \langle z_R|) | \Psi \rangle / \sqrt{p(z_R)}, \quad (2)$$

where \mathbb{I}_{AB} is the identity of subsystems A and B. Thus, the BPE for subsystems A and B can be defined as

$$\mathcal{E}_{\Psi,AB} := \{p(z_R), |\Psi_{AB}(z_R)\rangle\}. \quad (3)$$

To measure the correlation between subsystems A and B, we also define the EAE between A and B as

$$\bar{E}(A : B) := \sum_{z_R} p(z_R) S_A(z_R) = \sum_{z_R} p(z_R) S_B(z_R), \quad (4)$$

where $S_{A/B}(z_R)$ is the von Neuman entropy of subsystem A/B with respect to the state $|\Psi_{AB}(z_R)\rangle$. Here, both the BPE and EAE depend on the measurement bases. The maximum value of $\bar{E}(A : B)$ over the allowed measurement bases is the localizable entanglement [47, 48], which has been used to study ground-state quantum phase transitions and multipartite entanglements. In this work, we primarily utilize BPE and EAE to study entanglement phases, where we only consider a fixed basis. Our setting is suitable for numerical simulations and quantum simulators [44]. In the following discussion, for simplicity, we only consider $N_A = N_B = 1$, and r labels the distance between A and B, i.e., $\bar{E}(A : B) = \bar{E}(r)$.

Now we discuss relations between EAEs and the laws of entanglement entropies. We know that the localizable entanglements exhibit an exponential and a power-law decay for

gapped and gapless ground states of local systems [47, 48], respectively. Thus, intuitively, $\bar{E}(r)$ should exhibit an exponential decay for area-law entangled states, while it is power-law decay for states with subvolume-law entanglement. For volume-law entangled states, $\bar{E}(r)$ is expected to converge to a nonzero value when increasing r , i.e., $\lim_{r \rightarrow \infty} \bar{E}(r) \sim \text{const}$. To understand this, we can take a random state as an example, which is a typical volume-law entangled state describing quantum chaotic systems [49, 50]. For this state, $\mathcal{E}_{\Psi,AB}$ is nearly independent of measurement bases and the positions of A and B, and tends to be a Haar ensemble leading to $\bar{E}(r) \approx (\ln 2)/2$ for arbitrary r [44–46]. Therefore, BPE and EAE can identify different entanglement phases, see Fig. 1(b).

In conventional statistical physics, different phases can be identified by the behaviors of correlations of local order parameters. However, it remains a challenge to define a similar effective correlation function to describe entanglement phases. One potential candidate is quantum mutual information [51], which can characterize the quantum correlation of two subsystems. However, quantum mutual information between two local subsystems is akin to a connected correlation function, which tends to zero for both volume- and area-law entangled states [17], so it cannot distinguish between order and disorder phases. Here, EAE defined in Eq. (4) can be considered as an effective correlation function, enabling the mapping of entanglement phase transitions to conventional disorder-order phase transitions: (i) For a quantum state with area-law entanglement, $\bar{E}(r)$ exhibits an exponential decay when increasing the distance between two local subsystems, corresponding to a short-range correlated (disorder) phase. (ii) The correlation converges to a constant for large distance in the case of volume-law entanglement, corresponding to a long-range correlated (order) phase. (iii) For subvolume-law entanglement, the correlation exhibits a power-law decay implying a scale invariance, which generally describes critical systems.

Witness of measurement-induced phase transitions.—Since BPE and EAE can characterize the different laws of entanglement entropies, we now apply them to investigate MIPTs. The random Clifford circuit with local projective measurements is a paradigmatic model to study MIPTs, since it can be simulated efficiently on classical computers [52]. Here, we find that $\bar{E}(r)$ of stabilizer states can also be effectively calculated, and the details are presented in Supplemental Materials (SM) [53]. Thus, for concreteness, we take the measured stabilizer circuit model as an example to investigate BPE and EAE across a MIPT. The circuit diagram is shown in Fig. 1(c), where each time step contains two layers of gates and measurements. Each local two-qubit gate $\hat{U}_{j,j+1}$ is independently drawn from uniformly sampled Clifford group, and the probability of each projective measurement on the circuit is p . In addition, the measurement bases of the circuit and BPE are both z -component. We start from a trivial product state $|\Psi_0\rangle = |0\rangle^{\otimes L}$ with L being the system size.

Generally, the unitary quantum gates can produce the entanglement entropies, while the projected measurements can

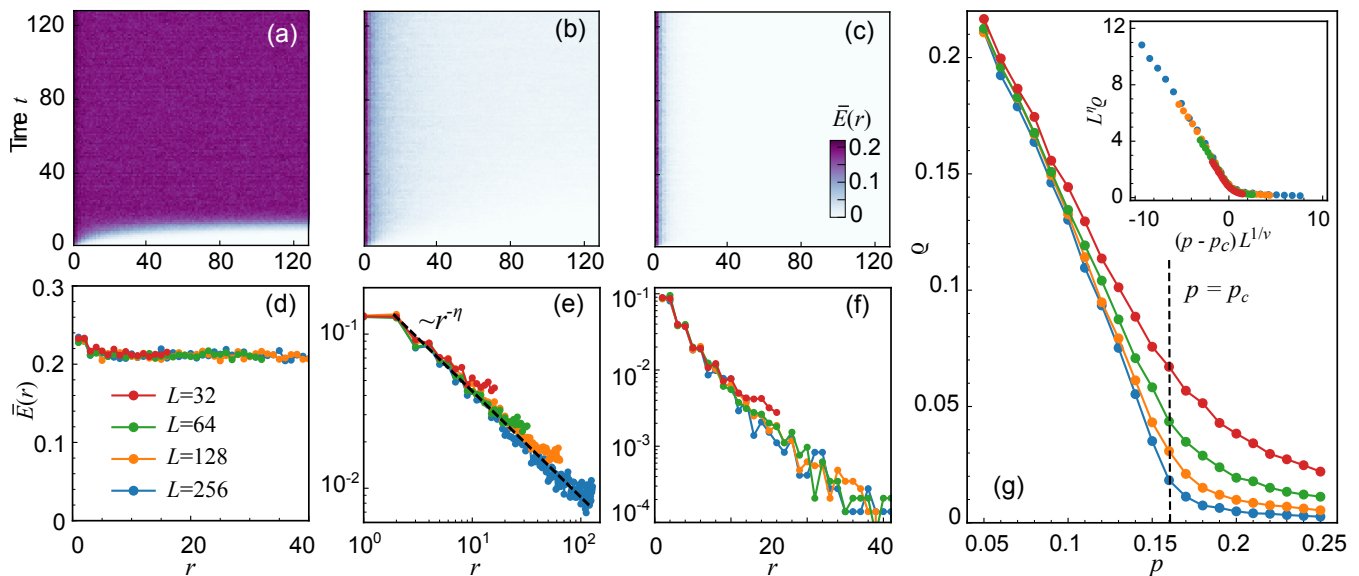


FIG. 2. The results of EAE for random Clifford circuits. The dynamics of $\bar{E}(r)$ for (a) $p = 0.05$, (b) $p = 0.16$, and (c) $p = 0.25$. The system size is $L = 256$. The scaling of $\bar{E}(r)$ at $t = 2L$ for (d) $p = 0.05$, (e) $p = 0.16$, and (f) $p = 0.25$. The black dashed line in (e) is for the fit: $\bar{E}(r) \sim r^{-\eta}$ with $\eta \approx 0.71$. (g) The integrated EAE ϱ versus p for different system sizes. The inset is a collapse of the data with the critical point $p_c \approx 0.16$ and exponent $\nu \approx 1.24$. We choose periodic boundary conditions. The sampling times are 10000 for $L = 32, 64, 128$, and 5000 for $L = 256$.

reduce the entanglements. Thus, when tuning the measurement probability p , there exists an entanglement phase transition with the critical point at $p_c \approx 0.16$ [13, 17, 22]. When $p < p_c$, the system is in an entangling phase with extensive entanglement entropies for steady states. When $p > p_c$, it is in a disentangling phase with area-law entanglement entropies. At the critical point, the entanglement entropies of steady states hold a sub-volume law.

Now we numerically study the behaviors of BPE and EAE across a MIPT. In Figs. 2(a-c), we present the dynamics of EAEs for different p . We can find that, for small p , the correlation can spread to the whole system, indicating extensive entanglement after a long-time evolution. However, for large p , there only exist short-range correlations during the dynamics, showing area-law entanglements. To further demonstrate this picture, we also present the results of $\bar{E}(r)$ for steady states ($t = 2L$). When $p < p_c$, $\bar{E}(r)$ can converge to a nonzero value for large distance, i.e., $\bar{E}(r \rightarrow \infty) \sim \text{const}$, see Fig. 2(d). At the critical point, we can find that EAE indeed holds a power-law decay, i.e., $\bar{E}(r) \sim r^{-\eta}$ with $\eta \approx 0.71$, see Fig. 2(e). When $p > p_c$, $\bar{E}(r)$ tends to exhibit an exponential decay, see Fig. 2(f). Our results show that the behaviors of $E(r)$ can diagnose the different entanglement phases of the measured stabilizer circuit, which is consistent with Fig. 1(b).

To further understand MIPT with EAE, we define the integrated EAE as

$$\varrho := \frac{1}{L} \sum_{r=1}^L \bar{E}(r). \quad (5)$$

Here, ϱ is in analogy with the squared magnetization in the Ising model, which is useful for identifying the magnetization

phase transition. We present the results of ϱ for steady states versus p in Fig. 2(g). Similar to the squared magnetization, in the order phase (small p), ϱ can be nonzero in the thermodynamic limit, while it tends to zero for the disorder phase (large p). Moreover, ϱ is also expected to satisfy the scaling ansatz

$$\varrho = L^{-\eta} F[(p - p_c)L^{1/\nu}]. \quad (6)$$

By data collapse, we can fix the critical point $p_c = 0.16$ and correlation length critical exponent $\nu \approx 1.24$ [see the inset in Fig. 2(g)], which is consistent with the results in Refs. [13, 17, 22]. Therefore, by introducing EAEs, MIPTs can indeed be described with the language of conventional disorder-order phase transitions. In the SM [53], we demonstrate that BPE and EAE can also identify MIPTs in measured Haar random circuits.

We also study the critical dynamic scaling of EAE in this system. Generally, the length scales in spatial (ξ) and temporal (τ) directions satisfy the relation: $\tau \sim \xi^z$, where z is the dynamical critical exponent. To identify the universal dynamics of EAE, we first need to obtain z . In previous literatures [13, 22], z is usually taken as 1. However, there has not been any reliable analytical or numerical results to verify $z = 1$ in this system [13, 22]. Here, we demonstrate that EAE can be used to obtain z . In analogy to conventional critical non-equilibrium systems, the dynamics of EAE is expected to satisfy the scaling ansatz [54]

$$\bar{E}(r, t, p) = t^{\theta-d/z} g[r/t^{1/z}, (p - p_c)t^{1/\nu z}], \quad (7)$$

where $d = 1$ is the spatial dimension, and θ is a universal critical exponent. Here, we can also define the k -moment of

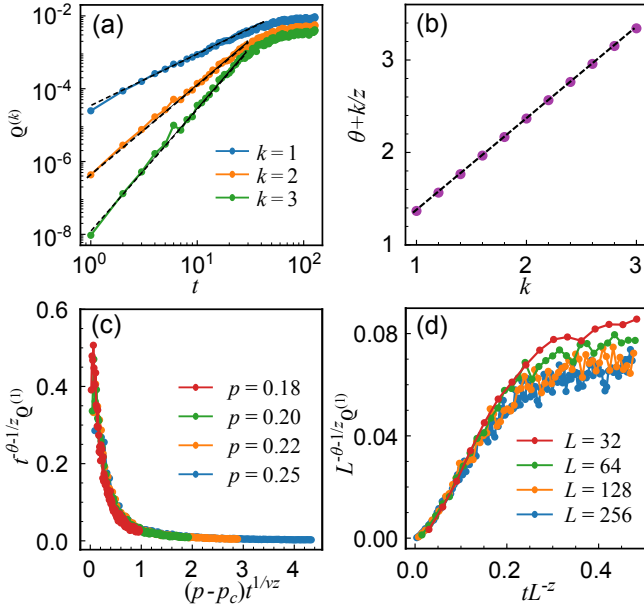


FIG. 3. Critical dynamic scaling. (a) The dynamics of $\varrho^{(k)}$ at the critical point with $L = 256$. The black dashed lines are linear fittings. (b) The scaling of $\varrho^{(k)}$ versus k . The black dashed line is linear fitting with $\theta \approx 0.38$ and $z \approx 1.01$. (c) The dynamics of $\varrho^{(1)}$ in the disentangling phase for different p with a fixed system size $L = 256$. (d) Finite-size scaling of $\varrho^{(1)}(t)$ at the critical point.

EAE as

$$\varrho^{(k)} := \frac{1}{L^{k+1}} \sum_r r^k \bar{E}(r), \quad (8)$$

where $\varrho = \varrho^{(k=0)}$. According to Eq. (7), we can obtain the dynamics of $\varrho^{(k)}$ by integrating r as

$$\varrho^{(k)}(t, p) = t^{\theta+k/z} G_k[(p-p_c)t^{1/\nu z}]. \quad (9)$$

Thus, in the thermodynamic limit $L \rightarrow \infty$ and at the critical point, the early-time dynamics of $\varrho^{(k)}$ satisfies

$$\varrho^{(k)}(t, p_c) = t^{\theta+k/z} G_k(0) \sim t^{\theta+k/z}. \quad (10)$$

In Fig. 3(a), we present the dynamics of $\varrho^{(k)}$ at the critical point for $L = 256$, where $\varrho^{(k)}$ indeed exhibits power-law increasing for early times. By fitting the corresponding exponents, we can obtain $z \approx 1.01$, and $\theta \approx 0.38$, see Fig. 3(b).

Now we can further verify the universal dynamics of $\varrho^{(k)}$. In Fig. 3(c), we plot the dynamics of $\varrho^{(1)}$ in the disorder phase. The perfect data collapse is consistent with the scaling ansatz in Eq. (9). In addition, at the critical point, the early-time dynamics of $\varrho^{(k)}$ can be generalized to the finite-size scaling form

$$\varrho^{(k)}(t) = L^{\theta+k/z} G(tL^{-z}). \quad (11)$$

In Fig. 3(d), we present the dynamics of $\varrho^{(1)}$ for different system sizes at the critical point, of which the results are consistent with Eq. (11).

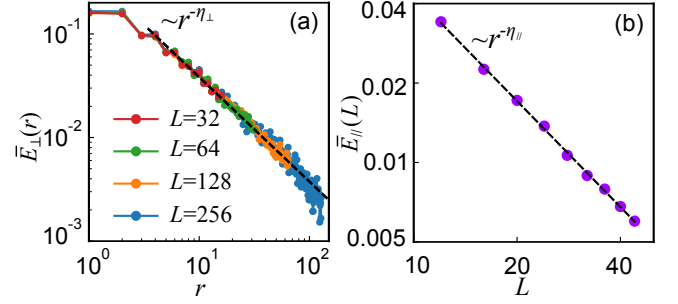


FIG. 4. Surface critical phenomena. (a) The scaling of EAEs between an edge site and a bulk edge. (b) The scaling of EAEs between two edge sites. The black dashed lines are linear fittings with $\eta_{\perp} \approx 1.02$ and $\eta_{\parallel} \approx 1.34$.

Now we apply EAE to identify surface criticality [55, 56], which requires open boundary conditions. We first consider an edge site as the subsystem A and a bulk site as the subsystem B, respectively, and label the corresponding EAE as $\bar{E}_{\perp}(r)$. In Fig. 4(a), we plot $\bar{E}_{\perp}(r)$ of steady states at the critical point. The results show that $\bar{E}_{\perp}(r)$ can also exhibit a power-law decay: $\bar{E}_{\perp}(r) \sim r^{-\eta_{\perp}}$, with $\eta_{\perp} \approx 1.02$.

Then we consider two edge sites as the subsystems A and B, respectively, and label the corresponding EAE as $\bar{E}_{\parallel}(L)$. In Fig. 4(b), we present numerical results of \bar{E}_{\parallel} of steady states versus the system size L at the critical point, where we can find that $\bar{E}_{\parallel}(L) \sim L^{-\eta_{\parallel}}$ with $\eta_{\parallel} \approx 1.34$. Therefore, similar to the correlation functions in convention phase transitions [55, 56], the bulk and surface critical exponents described by EAEs in this MIPT also satisfy the relation $\eta_{\perp} \approx (\eta + \eta_{\parallel})/2$.

Conclusion.—In summary, we have introduced the BPE and EAE to investigate entanglement phases. Our results demonstrate a one-to-one correspondence between EAE and the entanglement laws of quantum many-body wave functions. Using the measured stabilizer circuit as an example, we have illustrated the effectiveness of EAE in identifying MIPT. Specifically, we have shown that EAE enables us to obtain the universal scaling of dynamics and the surface critical exponents of MIPTs.

Our findings mainly offer twofold advantages: (i) EAEs can be regarded as a type of correlation functions, allowing us to apply concepts from conventional disorder-order phase transitions to understand entanglement phase transitions. Thus, our results enrich the study of entanglement phases. For instance, it enable us to study universal dynamic scaling and the surface criticality. (ii) Measuring EAEs in quantum simulators should be more scalable than measuring entanglement entropies. Thus, our results provide a convenient experimental method to study entanglement phases in quantum simulators. In addition, we anticipate the generalization of BPE and EAE to investigate other quantum many-body physics, such as quantum thermalization [50, 57–60] and many-body localizations [61–67].

Acknowledgments.—F. N. acknowledges partial support from: Nippon Telegraph and Telephone Corporation (NTT)

Research, the Japan Science and Technology Agency (JST) [via the Quantum Leap Flagship Program (Q-LEAP), and the Moonshot R&D Grant Number JPMJMS2061], the Asian Office of Aerospace Research and Development (AOARD) (via Grant No. FA2386-20-1-4069), and the Office of Naval Research (ONR) Global (via Grant No. N62909-23-1-2074).

-
- [1] M. M. Wilde, *Quantum information theory* (Cambridge university press, Cambridge, England, 2013).
- [2] J. Watrous, *The theory of quantum information* (Cambridge university press, Cambridge, England, 2018).
- [3] B. Cheng, X.-H. Deng, X. Gu, Y. He, G. Hu, P. Huang, J. Li, B.-C. Lin, D. Lu, Y. Lu, *et al.*, Noisy intermediate-scale quantum computers, *Frontiers of Physics* **18**, 21308 (2023).
- [4] B. Zeng, X. Chen, D.-L. Zhou, and X.-G. Wen, *Quantum information meets quantum matter* (Springer, 2019).
- [5] E. Fradkin, *Field theories of condensed matter physics* (Cambridge University Press, Cambridge, England, 2013).
- [6] L. Amico, R. Fazio, A. Osterloh, and V. Vedral, Entanglement in many-body systems, *Rev. Mod. Phys.* **80**, 517 (2008).
- [7] J. Eisert, M. Cramer, and M. B. Plenio, Colloquium: Area laws for the entanglement entropy, *Rev. Mod. Phys.* **82**, 277 (2010).
- [8] T. J. Osborne and M. A. Nielsen, Entanglement in a simple quantum phase transition, *Phys. Rev. A* **66**, 032110 (2002).
- [9] A. Osterloh, L. Amico, G. Falci, and R. Fazio, Scaling of entanglement close to a quantum phase transition, *Nature* **416**, 608 (2002).
- [10] G. Vidal, J. I. Latorre, E. Rico, and A. Kitaev, Entanglement in Quantum Critical Phenomena, *Phys. Rev. Lett.* **90**, 227902 (2003).
- [11] P. Calabrese and J. Cardy, Entanglement entropy and quantum field theory, *J. Stat Mech.* **2004**, P06002 (2004).
- [12] A. Polkovnikov, K. Sengupta, A. Silva, and M. Vengalattore, Colloquium: Nonequilibrium dynamics of closed interacting quantum systems, *Rev. Mod. Phys.* **83**, 863 (2011).
- [13] Y. Li, X. Chen, and M. P. A. Fisher, Quantum Zeno effect and the many-body entanglement transition, *Phys. Rev. B* **98**, 205136 (2018).
- [14] B. Skinner, J. Ruhman, and A. Nahum, Measurement-Induced Phase Transitions in the Dynamics of Entanglement, *Phys. Rev. X* **9**, 031009 (2019).
- [15] A. Chan, R. M. Nandkishore, M. Pretko, and G. Smith, Unitary-projective entanglement dynamics, *Phys. Rev. B* **99**, 224307 (2019).
- [16] M. Szyniszewski, A. Romito, and H. Schomerus, Entanglement transition from variable-strength weak measurements, *Phys. Rev. B* **100**, 064204 (2019).
- [17] Y. Li, X. Chen, and M. P. A. Fisher, Measurement-driven entanglement transition in hybrid quantum circuits, *Phys. Rev. B* **100**, 134306 (2019).
- [18] Y. Bao, S. Choi, and E. Altman, Theory of the phase transition in random unitary circuits with measurements, *Phys. Rev. B* **101**, 104301 (2020).
- [19] C.-M. Jian, Y.-Z. You, R. Vasseur, and A. W. W. Ludwig, Measurement-induced criticality in random quantum circuits, *Phys. Rev. B* **101**, 104302 (2020).
- [20] S. Choi, Y. Bao, X.-L. Qi, and E. Altman, Quantum Error Correction in Scrambling Dynamics and Measurement-Induced Phase Transition, *Phys. Rev. Lett.* **125**, 030505 (2020).
- [21] M. J. Gullans and D. A. Huse, Dynamical Purification Phase Transition Induced by Quantum Measurements, *Phys. Rev. X* **10**, 041020 (2020).
- [22] M. J. Gullans and D. A. Huse, Scalable Probes of Measurement-Induced Criticality, *Phys. Rev. Lett.* **125**, 070606 (2020).
- [23] A. Zabalo, M. J. Gullans, J. H. Wilson, S. Gopalakrishnan, D. A. Huse, and J. H. Pixley, Critical properties of the measurement-induced transition in random quantum circuits, *Phys. Rev. B* **101**, 060301 (2020).
- [24] X. Turkeshi, R. Fazio, and M. Dalmonte, Measurement-induced criticality in $(2+1)$ -dimensional hybrid quantum circuits, *Phys. Rev. B* **102**, 014315 (2020).
- [25] M. Szyniszewski, A. Romito, and H. Schomerus, Universality of Entanglement Transitions from Stroboscopic to Continuous Measurements, *Phys. Rev. Lett.* **125**, 210602 (2020).
- [26] M. Ippoliti, M. J. Gullans, S. Gopalakrishnan, D. A. Huse, and V. Khemani, Entanglement Phase Transitions in Measurement-Only Dynamics, *Phys. Rev. X* **11**, 011030 (2021).
- [27] M. Ippoliti and V. Khemani, Postselection-Free Entanglement Dynamics via Spacetime Duality, *Phys. Rev. Lett.* **126**, 060501 (2021).
- [28] O. Alberton, M. Buchhold, and S. Diehl, Entanglement Transition in a Monitored Free-Fermion Chain: From Extended Criticality to Area Law, *Phys. Rev. Lett.* **126**, 170602 (2021).
- [29] S. Sang and T. H. Hsieh, Measurement-protected quantum phases, *Phys. Rev. Res.* **3**, 023200 (2021).
- [30] M. Block, Y. Bao, S. Choi, E. Altman, and N. Y. Yao, Measurement-Induced Transition in Long-Range Interacting Quantum Circuits, *Phys. Rev. Lett.* **128**, 010604 (2022).
- [31] T. Minato, K. Sugimoto, T. Kuwahara, and K. Saito, Fate of Measurement-Induced Phase Transition in Long-Range Interactions, *Phys. Rev. Lett.* **128**, 010603 (2022).
- [32] T. Müller, S. Diehl, and M. Buchhold, Measurement-Induced Dark State Phase Transitions in Long-Ranged Fermion Systems, *Phys. Rev. Lett.* **128**, 010605 (2022).
- [33] S. Sharma, X. Turkeshi, R. Fazio, and M. Dalmonte, Measurement-induced criticality in extended and long-range unitary circuits, *SciPost Phys. Core* **5**, 023 (2022).
- [34] U. Agrawal, A. Zabalo, K. Chen, J. H. Wilson, A. C. Potter, J. H. Pixley, S. Gopalakrishnan, and R. Vasseur, Entanglement and Charge-Sharpener Transitions in $U(1)$ Symmetric Monitored Quantum Circuits, *Phys. Rev. X* **12**, 041002 (2022).
- [35] I. Poboiko, I. V. Gornyi, and A. D. Mirlin, Measurement-Induced Phase Transition for Free Fermions above One Dimension, *Phys. Rev. Lett.* **132**, 110403 (2024).
- [36] Y. Bao, M. Block, and E. Altman, Finite-Time Teleportation Phase Transition in Random Quantum Circuits, *Phys. Rev. Lett.* **132**, 030401 (2024).
- [37] C. Noel, P. Niroula, D. Zhu, A. Risinger, L. Egan, D. Biswas, M. Cetina, A. V. Gorshkov, M. J. Gullans, D. A. Huse, *et al.*, Measurement-induced quantum phases realized in a trapped-ion quantum computer, *Nature Physics* **18**, 760 (2022).
- [38] J. M. Koh, S.-N. Sun, M. Motta, and A. J. Minnich, Measurement-induced entanglement phase transition on a superconducting quantum processor with mid-circuit readout, *Nature Physics* **19**, 1314 (2023).
- [39] J. C. Hoke, M. Ippoliti, E. Rosenberg, *et al.*, Measurement-induced entanglement and teleportation on a noisy quantum processor, *Nature* **622**, 481 (2023).
- [40] I. Buluta and F. Nori, Quantum simulators, *Science* **326**, 108 (2009).
- [41] A. Trabesinger, Quantum simulation, *Nature Physics* **8**, 263 (2012).
- [42] I. M. Georgescu, S. Ashhab, and F. Nori, Quantum simulation, *Rev. Mod. Phys.* **86**, 153 (2014).

- [43] T. Brydges, A. Elben, P. Jurcevic, B. Vermersch, C. Maier, B. P. Lanyon, P. Zoller, R. Blatt, and C. F. Roos, Probing Rényi entanglement entropy via randomized measurements, *Science* **364**, 260 (2019).
- [44] J. Choi, A. L. Shaw, I. S. Madjarov, X. Xie, R. Finkelstein, J. P. Covey, J. S. Cotler, D. K. Mark, H.-Y. Huang, A. Kale, *et al.*, Preparing random states and benchmarking with many-body quantum chaos, *Nature* **613**, 468 (2023).
- [45] W. W. Ho and S. Choi, Exact Emergent Quantum State Designs from Quantum Chaotic Dynamics, *Phys. Rev. Lett.* **128**, 060601 (2022).
- [46] J. S. Cotler, D. K. Mark, H.-Y. Huang, F. Hernández, J. Choi, A. L. Shaw, M. Endres, and S. Choi, Emergent Quantum State Designs from Individual Many-Body Wave Functions, *PRX Quantum* **4**, 010311 (2023).
- [47] F. Verstraete, M. Popp, and J. I. Cirac, Entanglement versus Correlations in Spin Systems, *Phys. Rev. Lett.* **92**, 027901 (2004).
- [48] M. Popp, F. Verstraete, M. A. Martín-Delgado, and J. I. Cirac, Localizable entanglement, *Phys. Rev. A* **71**, 042306 (2005).
- [49] D. N. Page, Average entropy of a subsystem, *Phys. Rev. Lett.* **71**, 1291 (1993).
- [50] L. D'Alessio, Y. Kafri, A. Polkovnikov, and M. Rigol, From quantum chaos and eigenstate thermalization to statistical mechanics and thermodynamics, *Advances in Physics* **65**, 239 (2016).
- [51] M. M. Wolf, F. Verstraete, M. B. Hastings, and J. I. Cirac, Area Laws in Quantum Systems: Mutual Information and Correlations, *Phys. Rev. Lett.* **100**, 070502 (2008).
- [52] S. Aaronson and D. Gottesman, Improved simulation of stabilizer circuits, *Phys. Rev. A* **70**, 052328 (2004).
- [53] See Supplemental Material, .
- [54] A. Altland and B. D. Simons, *Condensed matter field theory*. (Cambridge University Press, Cambridge, England, 2010).
- [55] J. L. Cardy, Effect of boundary conditions on the operator content of two-dimensional conformally invariant theories, *Nuclear Physics B* **275**, 200 (1986).
- [56] J. L. Cardy, Conformal invariance and surface critical behavior, *Nuclear Physics B* **240**, 514 (1984).
- [57] J. M. Deutsch, Quantum statistical mechanics in a closed system, *Phys. Rev. A* **43**, 2046 (1991).
- [58] M. Srednicki, Chaos and quantum thermalization, *Phys. Rev. E* **50**, 888 (1994).
- [59] M. Srednicki, The approach to thermal equilibrium in quantized chaotic systems, *Journal of Physics A: Mathematical and General* **32**, 1163 (1999).
- [60] M. Rigol, V. Dunjko, and M. Olshanii, Thermalization and its mechanism for generic isolated quantum systems, *Nature* **452**, 854 (2008).
- [61] D. M. Basko, I. L. Aleiner, and B. L. Altshuler, Metal-insulator transition in a weakly interacting many-electron system with localized single-particle states, *Ann. Phys.* **321** (2006).
- [62] A. Pal and D. A. Huse, Many-body localization phase transition, *Phys. Rev. B* **82**, 174411 (2010).
- [63] J. A. Kjäll, J. H. Bardarson, and F. Pollmann, Many-Body Localization in a Disordered Quantum Ising Chain, *Phys. Rev. Lett.* **113**, 107204 (2014).
- [64] D. A. Huse, R. Nandkishore, and V. Oganesyan, Phenomenology of fully many-body-localized systems, *Phys. Rev. B* **90**, 174202 (2014).
- [65] M. Serbyn and J. E. Moore, Spectral statistics across the many-body localization transition, *Phys. Rev. B* **93**, 041424 (2016).
- [66] R. Nandkishore and D. A. Huse, Many-Body Localization and Thermalization in Quantum Statistical Mechanics, *Annual Review of Condensed Matter Physics* **6**, 15 (2015).
- [67] D. A. Abanin, E. Altman, I. Bloch, and M. Serbyn, Colloquium: Many-body localization, thermalization, and entanglement, *Rev. Mod. Phys.* **91**, 021001 (2019).

SUPPLEMENTAL MATERIALS:
IDENTIFYING ENTANGLEMENT PHASES WITH BIPARTITE PROJECTED ENSEMBLES

A. Ensemble averaged entanglements for Stabilizer Codes

Here we present details about how to calculate ensemble averaged entanglements (EAEs) of stabilizer states. Consider a codeword $|\psi\rangle$ determined by the stabilizer group

$$\mathcal{S} = \{\hat{g}_1, \hat{g}_2, \dots, \hat{g}_L : \hat{g}_\alpha |\psi\rangle = |\psi\rangle\}, \quad (\text{S1})$$

where L is the number of qubits, \hat{g}_α is a Pauli string operator satisfying $[\hat{g}_\alpha, \hat{g}_\beta] = 0$. Now, for the wave function $|\psi\rangle$, we perform a projected measurement of the j -th qubit onto the z component.

Firstly, we consider a simple case, where $|\psi\rangle$ is the eigenstate of $\hat{\sigma}_j^z$, i.e., $[\hat{g}_\alpha, \hat{\sigma}_j^z] = 0$ for all α . Thus, the measurement result is certain, and the wave function remains invariant after the projected measurement.

Secondly, we consider the case when $|\psi\rangle$ is not an eigenstate of $\hat{\sigma}_j^z$. Here, without loss of generality, we consider $[\hat{g}_1, \hat{\sigma}_j^z]_+ = 0$, while $[\hat{g}_\alpha, \hat{\sigma}_j^z] = 0$ for $\alpha \neq 1$. This can always be satisfied. For instance, if there exists \hat{g}_β ($\beta \neq 1$) that satisfies $[\hat{g}_\beta, \hat{\sigma}_j^z]_+ = 0$, we can rewrite \hat{g}_β as

$$\hat{g}_\beta \mapsto \hat{g}_1 \hat{g}_\beta, \quad (\text{S2})$$

and the new \hat{g}_β commute with $\hat{\sigma}_j^z$. Now the measurement result can be either $+1$ or -1 with equal probabilities. If the measurement result is $+1$, the wave function collapses to

$$|\psi\rangle \mapsto |\tilde{\psi}_+\rangle = \frac{1 + \sigma_j^z}{2} |\psi\rangle. \quad (\text{S3})$$

We can also find that $|\tilde{\psi}_+\rangle$ satisfies

$$\begin{aligned} \hat{g}_\alpha |\tilde{\psi}_+\rangle &= |\tilde{\psi}_+\rangle \quad (\alpha \neq 1), \\ \sigma_j^z |\tilde{\psi}_+\rangle &= |\tilde{\psi}_+\rangle. \end{aligned} \quad (\text{S4})$$

Thus, the new codeword $|\tilde{\psi}_+\rangle$ is determined by the following stabilizer group

$$\tilde{\mathcal{S}}_+ = \{\hat{g}_1 = \hat{\sigma}_j^z, \hat{g}_2, \dots, \hat{g}_L : \hat{g}_\alpha |\tilde{\psi}_+\rangle = |\tilde{\psi}_+\rangle\}, \quad (\text{S5})$$

Similarly, if the measurement result is -1 , then the wave function after the projected measurement, labeled by $|\tilde{\psi}_-\rangle$, is determined by the following stabilizer group

$$\tilde{\mathcal{S}}_- = \{\hat{g}_1 = -\hat{\sigma}_j^z, \hat{g}_2, \dots, \hat{g}_L : \hat{g}_\alpha |\tilde{\psi}_-\rangle = |\tilde{\psi}_-\rangle\}. \quad (\text{S6})$$

Thus, the difference between $\tilde{\mathcal{S}}_+$ and $\tilde{\mathcal{S}}_-$ is just that the corresponding \hat{g}_1 has the opposite sign.

Note that the entanglement entropy of a codeword $|\psi\rangle$ is independent of the signs of \hat{g}_α . Thus, $\tilde{\mathcal{S}}_+$ and $\tilde{\mathcal{S}}_-$ have the same entanglement entropies. Generalizing to the case of joint projected measurements of many qubits, we can conclude that the entanglement entropy of a codeword after the measurements is independent of the measurement results. Therefore, for a codeword $|\psi\rangle$, we consider the bipartite projected ensemble (BPE) with respect to the z -component basis as

$$\mathcal{E}_{\psi, AB} := \{p(z_R), |\Psi_{AB}(z_R)\rangle\}. \quad (\text{S7})$$

The von Neuman entropy of subsystem A/B for the state $|\Psi_{AB}(z_R)\rangle$ is z_R -independent. Therefore, when calculating the EAE of $\mathcal{E}_{\psi, AB}$, we can first perform a projected measurement of the subsystem R. Then calculate the von Neuman entropy of subsystem A/B, which is the EAE of $\mathcal{E}_{\psi, AB}$.

B. Haar random quantum circuits with projective measurements

In the main text, we have applied BPE and EAE to investigate MIPT in the measured stabilizer circuits. In this section, we apply BPE and EAE to study MIPT in Haar random quantum circuits with projective measurements. The numerical results are shown in Fig. S1 with periodic boundary conditions. We find that EAE can indeed identify the MIPT of Haar random quantum circuits with projective measurements, and the critical point is consistent with Ref. [23]. We also calculate the critical exponents as $\nu \approx 1.4$ and $\eta \approx 0.45$.

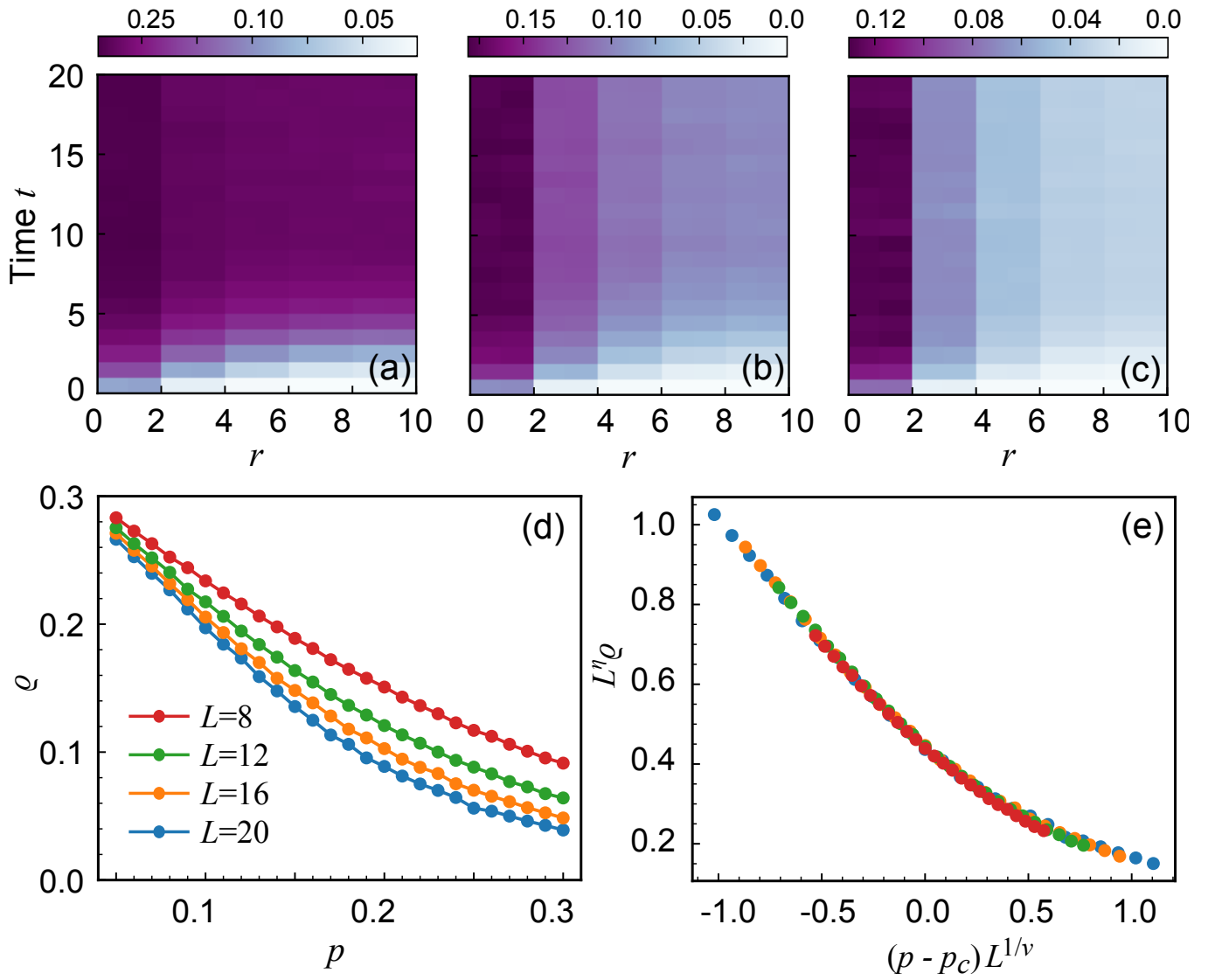


FIG. S1. The results of EAE for Haar random circuits. The dynamics of $\bar{E}(r)$ for (a) $p = 0.05$, (b) $p = 0.17$, and (c) $p = 0.25$. The system size is $L = 20$. (d) The integrated EAE ρ of steady states versus p for different system sizes. (e) Data collapse of (d) using Eq. (6) with the critical point $p_c \approx 0.17$ and exponents $\nu \approx 1.4$ and $\eta \approx 0.45$.